



## STRONG GROUND MOTION SIMULATIONS OF THE 1923 GREAT KANTO EARTHQUAKE IN THE TOKYO METROPOLITAN AREA BASED ON THE STRONG MOTION GENERATION AREA

F. Suzuki<sup>(1)</sup>, K. Kato<sup>(2)</sup>, T. Watanabe<sup>(3)</sup>, Y. Tomozawa<sup>(4)</sup>

<sup>(1)</sup> Deputy Manager, Earthquake & Soil Dynamics Research Department, Kobori Research Complex Inc., [fumino-suzuki@kobori-takken.co.jp](mailto:fumino-suzuki@kobori-takken.co.jp)

<sup>(2)</sup> Deputy Director, Kobori Research Complex Inc., [katokenichi@kobori-takken.co.jp](mailto:katokenichi@kobori-takken.co.jp)

<sup>(3)</sup> Assistant General Manager, Earthquake & Soil Dynamics Research Department, Kobori Research Complex Inc., [watanabe@kobori-takken.co.jp](mailto:watanabe@kobori-takken.co.jp)

<sup>(4)</sup> Manager, Earthquake & Soil Dynamics Research Department, Kobori Research Complex Inc., [tomozawy@kobori-takken.co.jp](mailto:tomozawy@kobori-takken.co.jp)

### Abstract

The 1923 Great Kanto earthquake, which is one of the most devastating earthquakes in history, caused serious damage to the Tokyo metropolitan area. Given that similar earthquakes are likely to occur in the future, it is important to appropriately simulate the strong ground motions caused by large earthquakes to obtain data for the improvement of disaster prevention measures. In this study, the strong ground motions of the 1923 Great Kanto earthquake in the Tokyo metropolitan area were simulated using the stochastic Green's function.

Source characteristics were modeled using the strong motion generation area (SMGA), which was developed from both the short-period energy distribution and short-period spectral level of this event given by Kanda and Kato (2019) [1]. The short-period energy distribution was estimated by inversion analysis by using the seismic intensity distribution evaluated from the collapse rate of wooden houses [2]. The six SMGAs are located along the subducting Philippine Sea plate. The short-period spectral level for each SMGA was evaluated on the basis of the relation between the seismic moment and area.

Path and site characteristics were modeled on the basis of the inhomogeneous attenuation structure and the empirical amplification factors given by Tomozawa and Kato [3]. These were estimated by block inversion analysis by using the strong ground motion data of recent earthquakes. Furthermore, Q-values are given according to the path connecting each SMGA and each simulation site. The empirical site amplification factors from the seismic bedrock to the surface are provided under linear assumption in the Fourier spectral domain.

The validity of the simulation results was verified by comparing them with the observed seismic intensity distribution provided by Moroi and Takemura [2]. Although the simulation and observation sites are not exactly in the same location, both seismic intensities are essentially consistent.

The acceleration waveforms and response spectra of the simulation were shown for a small number of sites that have relatively lower amplification factors than other sites and exhibit few nonlinear effects. Their peak ground acceleration was approximately 200 to 1000 cm/s<sup>2</sup>, and their response spectral levels, which were measured at periods of approximately one to two seconds, are approximately 30 to 100 cm/s.

To simulate additional details within a wide area, studies on the nonlinear effects and spatial interpolation of empirical amplification factors are needed.

*Keywords: the 1923 Great Kanto earthquake; SMGA; seismic intensity; strong ground motion simulation*



## 1. Introduction

The 1923 Great Kanto earthquake, which is one of the most devastating earthquakes in history, caused significant damage to the Tokyo metropolitan area. The earthquake was an interplate event along the Sagami trough, which is where the subducting Philippine Sea plate is located. To prevent the likelihood of similar events from occurring in the future, appropriate disaster prevention strategies need to be developed by simulating the strong ground motions caused by large earthquakes. Short-period strong ground motions were not recorded during the 1923 Great Kanto earthquake. However, seismic intensity data can be used for source modeling short-period strong motion simulations. In Moroi and Takemura [2], seismic intensity distribution that uses the collapse rate of wooden houses caused by the 1923 Great Kanto earthquake was evaluated. Furthermore, by using seismic intensity data, Kanda and Kato [1] estimated the short-period energy distribution that radiated from the fault plane by inversion analysis. The research results indicate six strong motion generation areas (SMGAs) based on short-period energy distribution. Kanda and Kato [1] also estimated the short-period level, which is a flat level of an acceleration source spectrum, on the basis of the relationship between seismic intensity levels and the short-period levels of recent earthquakes.

In addition to source characteristics, path characteristics and site-specific amplification factors are important for conducting strong motion simulations. By using a large selection of recent observation records, Tomozawa and Kato [3] estimated the inhomogeneous attenuation structure and empirical amplification factors in the Kanto region by using block inversion analysis within the Fourier spectral domain.

In this study, the strong ground motions of the 1923 Great Kanto earthquake in the Tokyo metropolitan area were simulated using source, path, and site characteristics on the basis of the results of Kanda and Kato [1] and Tomozawa and Kato [3]. Strong motion waveforms were generated using the stochastic Green's function. The validity of the simulation results was verified by comparing the simulated seismic intensity distribution with the observed seismic intensity distribution. Acceleration waveforms and response spectral levels were also discussed.

## 2. Simulation methodology

Fig. 1 provides the simulation flowchart of this study. Source characteristics were modeled by using the six SMGAs developed via seismic intensity inversion analysis [1]. Path and site characteristics were modeled on the basis of the inhomogeneous attenuation structure and empirical amplification factors [3]. Strong motion waveforms were calculated using the stochastic Green's function on the basis of the synthesis method of Irikura [4]. An acceleration time series for each subfault was artificially generated on the basis of Boore [5] by considering the path and site characteristics mentioned above. These simulations generated the acceleration waveforms of strong ground motions and seismic intensities ( $I_{JMA}$ ), and response spectra were calculated by the resulting waveforms.

### 2.1 Source characteristics

Table 1 shows the fault parameters of the SMGA model, and Fig. 2 shows the locations of SMGAs as blue rectangles and the short-period energy distribution that radiated from the fault plane [1].

The short-period level of each SMGA  $A_i$  (subscript “ $i$ ” represents the SMGA number) was calculated from the short-period level of entire fault  $A$ , the seismic moment of each SMGA  $M_{0i}$ , and the area of each  $S_i$  in [1] by using the following relationship. First, assuming that the  $\omega$ -square model was applicable for modeling each SMGA,  $A_i$  is expressed as follows:

$$A_i = (2\pi f_{ci})^2 M_{0i}, \quad (1)$$

where  $f_{ci}$  is the corner frequency of each SMGA. Second, by assuming that Brune's model [6, 7] and the circular crack model [8] were applicable for the modeling of each SMGA,  $f_{ci}$  is expressed by the radius  $r_i$  and stress drop  $\Delta\sigma_i$  of each SMGA:

$$2\pi f_{ci}^2 = 4\pi V_s^2 r_i \frac{\Delta\sigma_i}{M_{0i}} = \frac{7\pi V_s}{4 r_i^2}, \quad (2)$$

where  $V_s$  is the shear wave velocity. The proportional relationship is expressed as follows:



$$f_{c_i}^2 \propto \frac{1}{r_i^2} \propto \frac{1}{S_i} \quad (3)$$

By combining Eqs. (1) and (3), the following is obtained:

$$A_i \propto \frac{M_{0_i}}{S_i} \quad (4)$$

The relationship between  $A$  and  $A_i$  is expressed as follows:

$$A^2 = \sum_i A_i^2 \quad (5)$$

By employing Eqs. (4) and (5),  $A_i$  is obtained as follows:

$$A_i = A \times \frac{M_{0_i}/S_i}{\sqrt{\sum (M_{0_i}/S_i)^2}} \quad (6)$$

Therefore, each  $A_i$  was modeled from  $A$ , as shown in Eq. (6).

Each SMGA was converted into a rectangular model that encompasses the area being studied. The strike and dip angle were set along the subducting Philippine Sea plate [9]. The background area was not considered. The  $V_s$  and density  $\rho$  in the source area were 3.53 km/s and 2.7 g/cm<sup>3</sup> [10], and  $f_{\max}$  was 13.5 Hz [11]. The radiation pattern coefficient was 0.63, which is the average across the entire focal sphere [12]. The rupture velocity  $V_r$  was 3.0 km/s [13]. The rise time for each SMGA  $\tau_i$  was estimated from the relationship  $\tau_i = 0.5S_i^{1/2}/V_r$ . The rupture starting point of the entire fault was set on the subfault of SMGA4, which was closest to the hypocenter the fault of Sato *et al.* [14]. The rupture of each SMGA was assumed to be the multi-hypocenter.

## 2.2 Path characteristics

Fig. 3 shows the inhomogeneous attenuation structure of the continental plate and the Q-values of each block estimated from the strong motion records in the Kanto region [3]. The method did not require assuming that the region is divided in advance. The divided region was estimated on the basis of the statistical test. Once the statistically significant level was satisfied in each block (on the basis of the minimum block size assumed), the inhomogeneous attenuation structure could be estimated on the basis of the resolution according to the number of data. The average Q-value in the Kanto area was estimated by Kinoshita [15] as  $100f^{0.7}$  ( $f$  = frequency). B10 was slightly higher than  $100f^{0.7}$ , and B12 and B19 were slightly lower than  $100f^{0.7}$ . In the current study, an equivalent Q-value that connects the path between each SMGA and simulation site was applied to reflect the characteristics of the simulations.

## 2.3 Site amplification

Fig. 4 shows the empirical amplification factors of the K-NET and KiK-net (surface) [16] sites in the Kanto region, which were estimated from the inhomogeneous attenuation structure mentioned above [3]. The colored lines indicate the seven sites with relatively lower amplification factors than other sites. In the current study, the empirical amplification factors from the seismic bedrock to the surface were used under linear assumption.

## 2.4 Other assumptions for simulation

The envelope function for the acceleration time series of each subfault is given by Satoh *et al.* [17]. Different random phases were assigned to the N-S and E-W horizontal components. In the synthesis method, random fluctuations were assigned to rupture fronts, with random numbers provided in five cases. The target frequency ranged from 0.2 to 20 Hz, similar to that as Tomozawa and Kato [3].

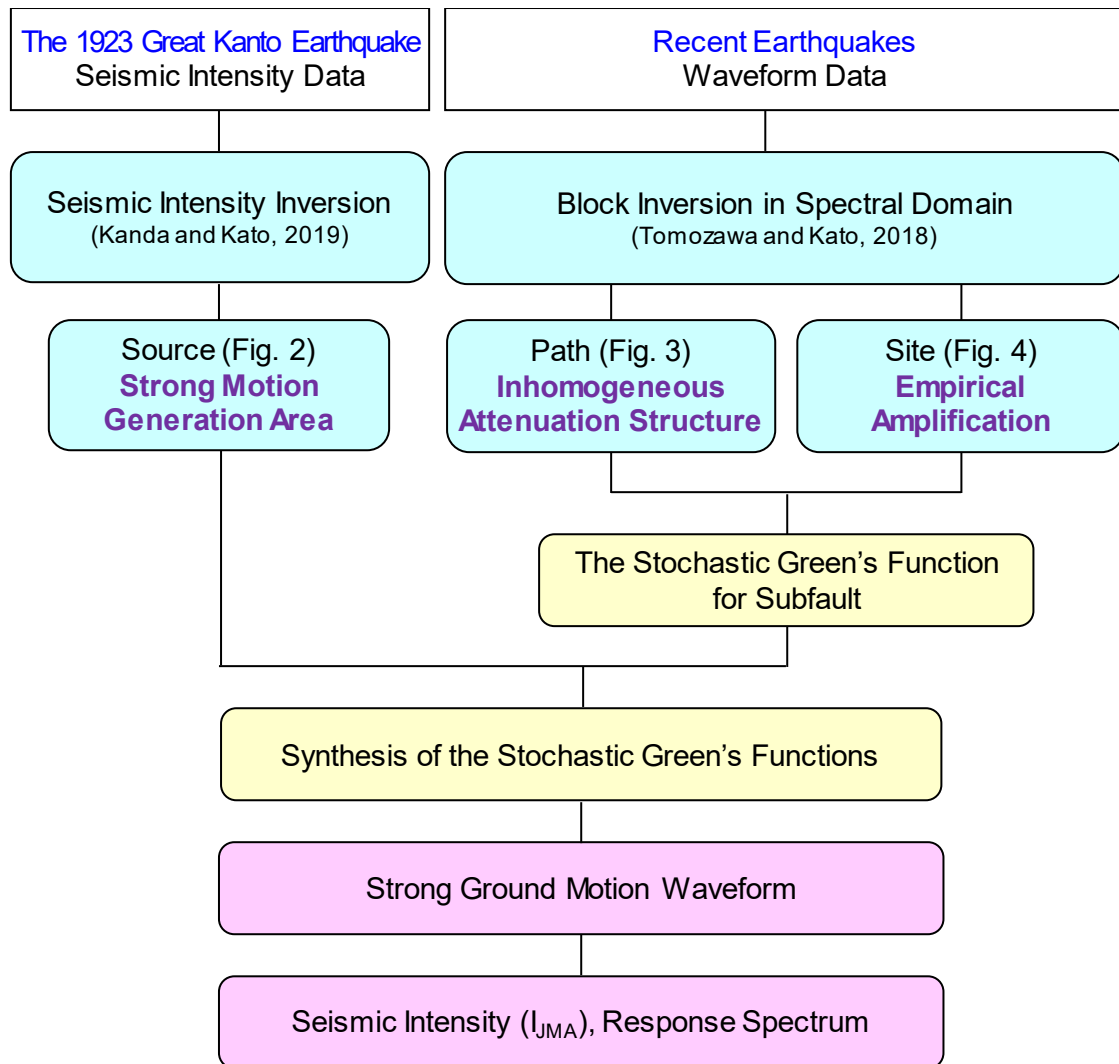


Fig. 1 – Simulation flowchart.



Table 1 – Fault parameters of SMGAs.

Parameter		Value		References				
Moment magnitude	$M_W$	7.9		Kanda and Kato (2019)				
Seismic moment	$M_0$ (Nm)	8.91E+20		Kanda and Kato (2019)				
Short period level	$A$ (Nm/s <sup>2</sup> )	4.66E+19		Kanda and Kato (2019)				
Area	$S$ (km <sup>2</sup> )	1871		$S = \sum S_i$				
S-wave velocity	$V_s$ (km/s)	3.53		HERP (2009)				
Density	$\rho$ (g/cm <sup>3</sup> )	2.7		HERP (2009)				
Rigidity	$\mu$ (N/m <sup>2</sup> )	3.36E+10		$\mu = \rho V_s^2$				
Rupture velocity	$V_r$ (km/s)	3.0		Kato <i>et al.</i> (2013)				
fmax	$f_{max}$ (Hz)	13.5		$P(f) = 1 / (1 + (f/f_{max})^{8.2})^{1/2}$ , Satoh <i>et al.</i> (1994a)				
Number of SMGA		#1	#2	#3	#4	#5	#6	
Seismic moment	$M_{0i}$ (10 <sup>20</sup> Nm)	1.81	1.77	1.64	1.08	1.46	1.17	Kanda and Kato (2019)
Area	$S_i$ (km <sup>2</sup> )	400	324	441	225	256	225	Kanda and Kato (2019)
Short period level	$A_i$ (10 <sup>19</sup> Nm/s <sup>2</sup> )	1.76	2.10	1.43	1.85	2.20	2.00	$A_i = A \times (M_{0i}/S_i) / [\sum (M_{0i}/S_i)^2]^{1/2}$
Top of depth	$h$ (km)	9.5	3.2	11.8	5.4	28.2	14.8	Along the top depth of the Philippine Sea plate
Strike	$\theta$ (°)	294	326	313	300	291	282	(Disaster Management in Japan, 2013)
Dip	$\delta$ (°)	17	19	17	25	15	20	
Rise time	$\tau_i$ (s)	3.3	3.0	3.5	2.5	2.7	2.5	$\tau_i = S_i^{1/2} / (2V_r)$

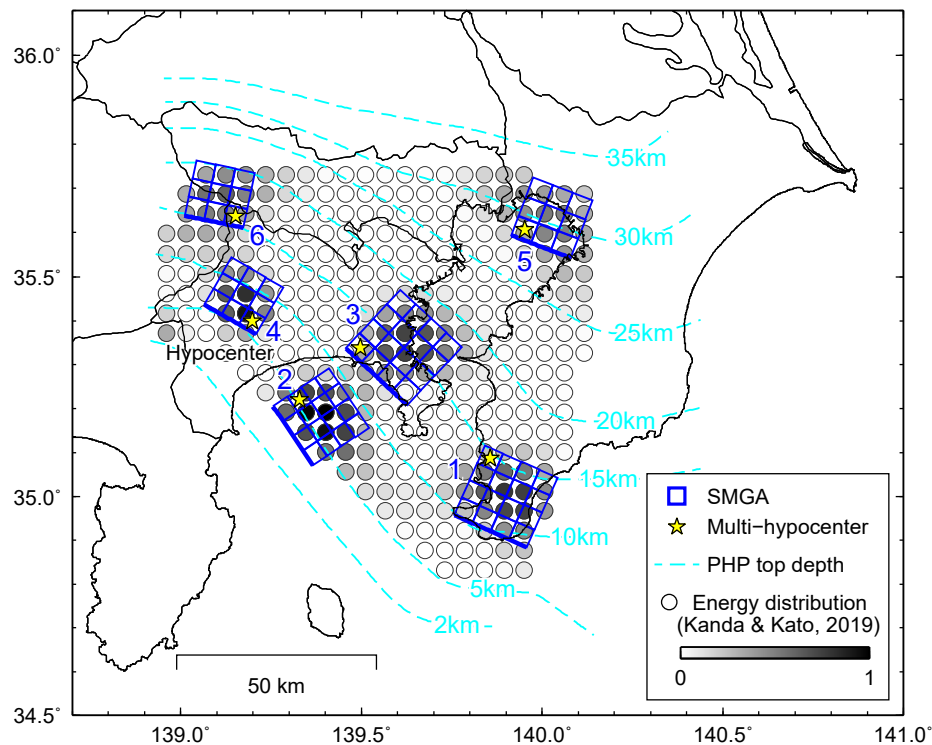


Fig. 2 – SMGA locations. The blue rectangles denote the SMGAs used in this simulation. The circles indicate the short-period energy distribution that radiated from the fault plane [1].

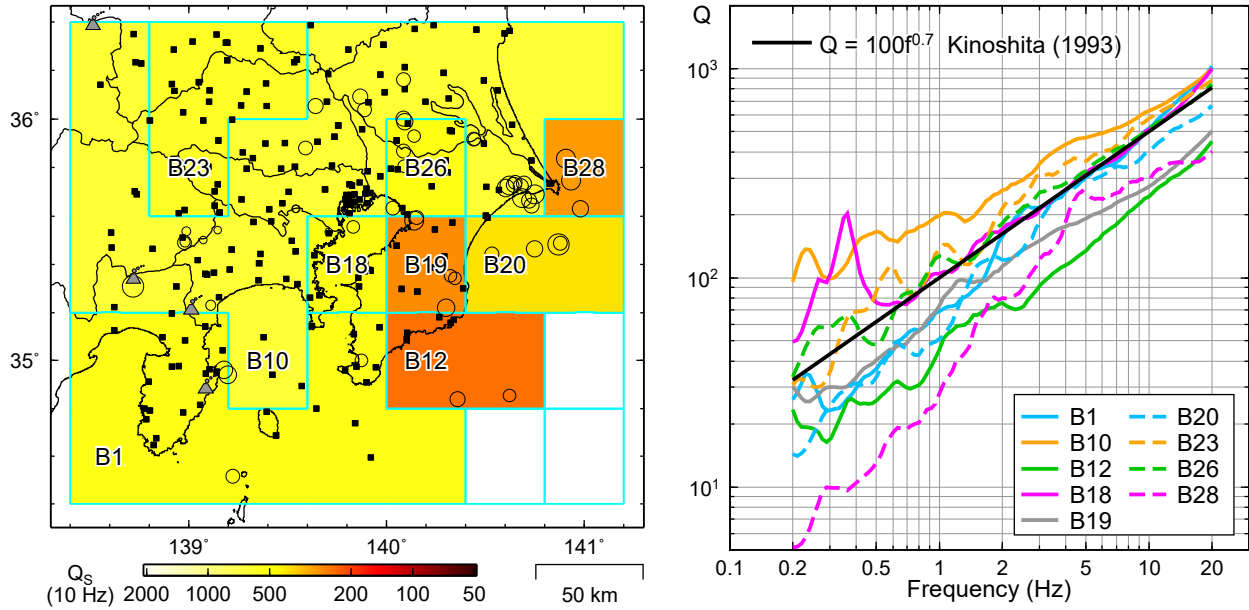


Fig. 3 – Inhomogeneous attenuation structure of the continental plate in the Kanto region [3]. Area division (left) and Q-values of each frequency (right).

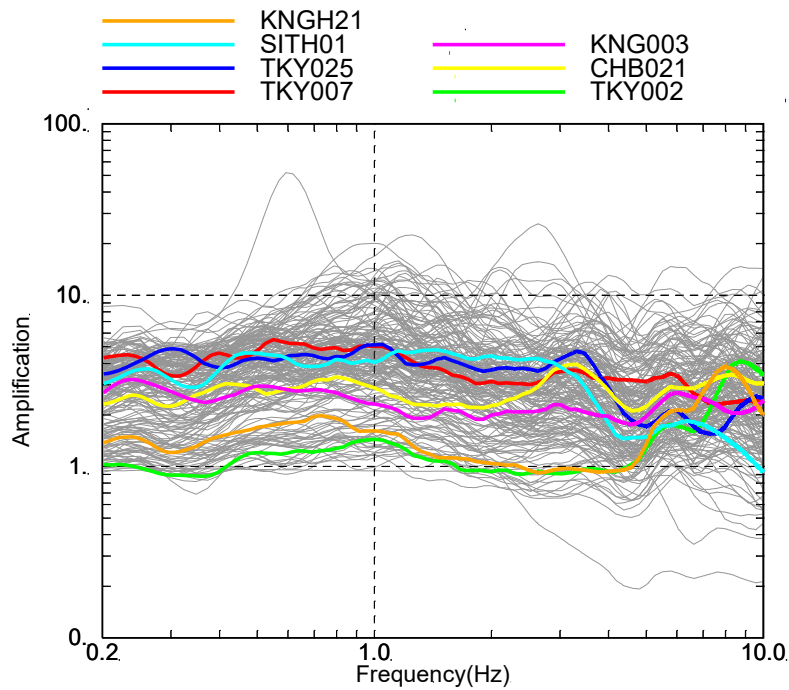


Fig. 4 – Empirical amplification factors of the K-NET and KiK-net (surface) sites in the Kanto region [3]. The colored lines indicate the seven sites with relatively lower amplification than other sites.



### 3. Simulation results

#### 3.1 Seismic intensity of the simulation results

Fig. 5 shows the seismic intensity distribution of the simulation (upper image) and observation (lower image) based on Moroi and Takemura [2]. The seismic intensities are expressed according to the Japanese Meteorological Agency scale, namely, “ $I_{JMA}$ ,” which includes 10 classes (0, 1, 2, 3, 4, 5<sup>-</sup>, 5<sup>+</sup>, 6<sup>-</sup>, 6<sup>+</sup>, and 7). The  $I_{JMA}$  of the simulation results were calculated by averaging the front fluctuations of the five rupture cases, as shown in the synthesized method of Irikura [4].

In the simulation results,  $I_{JMA}$ -7 sites were distributed in the southern Kanagawa and southern Chiba Prefectures. Furthermore,  $I_{JMA}$ -6<sup>+</sup> or 6<sup>-</sup> sites were widely distributed in Tokyo, Chiba, Saitama, Kanagawa, Ibaraki, Yamanashi, and Shizuoka Prefectures.

The site amplification factors in this study were based on the records of small or medium earthquakes. Therefore, these site amplification factors were applied to linear range and nonlinear site characteristics under large ground motions were not considered. Detailed studies of nonlinear site effects for the results of this simulation is a topic for future research.

The validity of the simulation results was checked by comparing them with the observed seismic intensity distribution (Fig. 5, lower image). In the simulations mentioned above, the  $I_{JMA}$  7, 6<sup>+</sup>, and 6<sup>-</sup> distribution trends were generally consistent with the observed distribution trends. Seven sites (indicated by arrows in Fig. 5 [upper image]) had relatively lower amplification factors than the remaining sites (shown in color in Fig. 4) and appeared to have the little nonlinear effects. For the seven sites, Table 2 shows a comparison of  $I_{JMA}$  between the simulations and observations. The observation sites were located near the simulation sites but not exactly in the same location. Sites TKY002, CHB021, KNG003, and KNGH21 were located near the SMGA (fault distances within 20 km), and sites TKY007, TKY025, and SITH01 were located slightly away from the SMGA (fault distances above 30 km). At both locations, the simulations and observations were essentially consistent. Considering that the simulation and observation sites were not exactly in the same location, it was difficult to compare both in great detail. To evaluate the same locations as the observation sites, spatial interpolation studies that use empirical amplification factors are required.

#### 3.2 Waveforms and response spectra level

The details of the simulation results are discussed below for the seven sites that had relatively lower amplification factors. Fig. 6 shows an example of the acceleration waveforms for one of the five rupture fluctuation cases. The sites near the SMGA (TKY002, CHB021, KNG003, and KNGH21) had a large peak ground acceleration (PGA) of approximately 600 to 1000 cm/s<sup>2</sup> at relatively short durations of approximately 10 to 15 seconds. The sites that are slightly further from the SMGA (TKY007, TKY025, and SITH01) had a PGA of approximately 200 to 400 cm/s<sup>2</sup> with longer durations of approximately 40 seconds. Among the seven sites, KNGH21 had the largest PGA with a value of approximately 1000 cm/s<sup>2</sup>. Fig. 7 shows the pseudo velocity response spectra, which are calculated as the geometric mean of the N-S and E-W components from the five cases. At periods of approximately one to two seconds, sites TKY007, TKY025, CHB021, KNG003, and KNGH21 showed significant responses of approximately 100 cm/s, whereas sites TKY002 and SITH01 showed relatively minor responses of approximately 30 to 70 cm/s. The peak of KNGH21 and TKY002 at a period of approximately 0.1 seconds was affected by their empirical amplification factors. Finally, CHB021 had the highest seismic intensity at 6<sup>+</sup> and exhibited the largest response among the seven sites at periods of approximately 0.2 to 1 second.

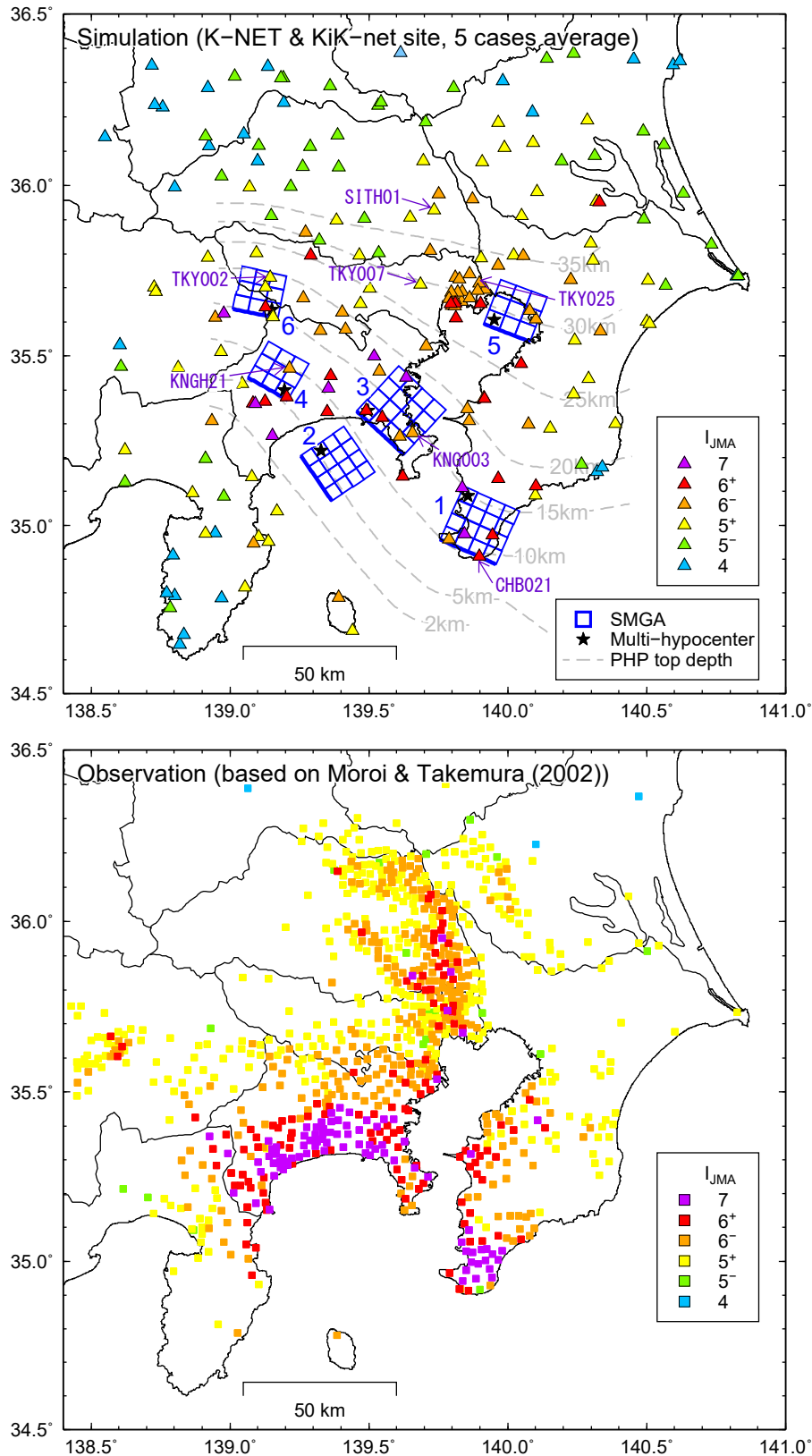


Fig. 5 – Seismic intensity  $I_{JMA}$  distributions of the 1923 Great Kanto earthquake in the Tokyo metropolitan area; simulation (top image) and observation (lower image) data. The seven sites indicated by arrows in the simulation results are shown in color in Fig. 4, and have relatively lower amplification factors than other sites.



Table 2 – Comparison of  $I_{JMA}$  between simulations and observations (near the simulation site).

	TKY007	TKY002	TKY025	CHB021	SITH01	KNG003	KNGH21
Simulation	5 <sup>+</sup>	5 <sup>+</sup>	6 <sup>-</sup>	6 <sup>+</sup>	5 <sup>+</sup>	6 <sup>-</sup>	6 <sup>-</sup>
Observation	5 <sup>+</sup> - 6 <sup>-</sup>	5 <sup>+</sup> - 6 <sup>-</sup>	5 <sup>+</sup> - 6 <sup>+</sup>	5 <sup>-</sup> - 6 <sup>+</sup>	5 <sup>+</sup> - 6 <sup>+</sup>	6 <sup>-</sup> - 7	6 <sup>-</sup> - 6 <sup>+</sup>

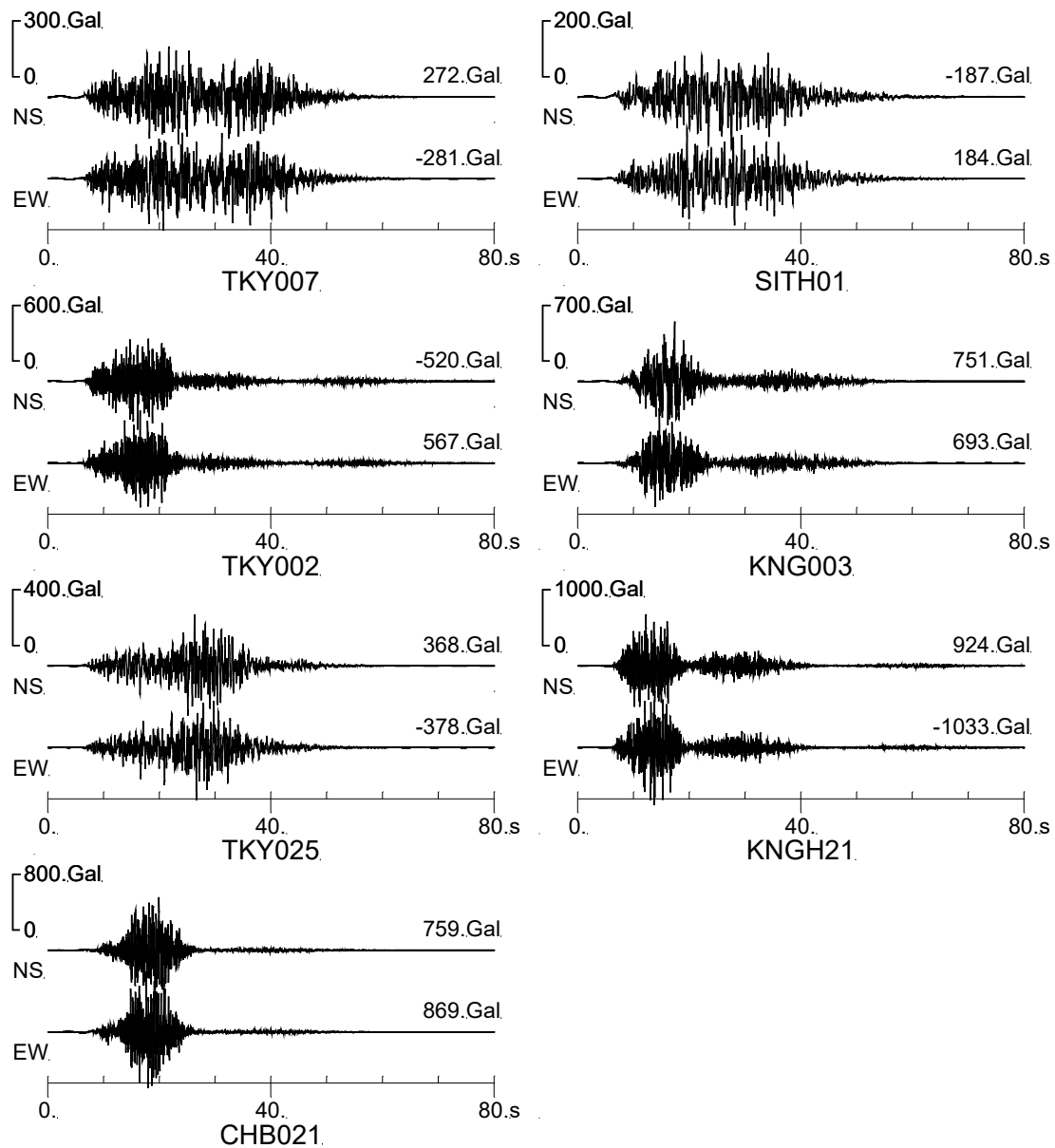


Fig. 6 – Acceleration waveforms of strong ground motion simulations. The seven sites are shown in color in Fig. 4, and these sites have relatively lower amplification factors than other sites. The numbers indicated at the upper right of the waveforms indicate the PGA.

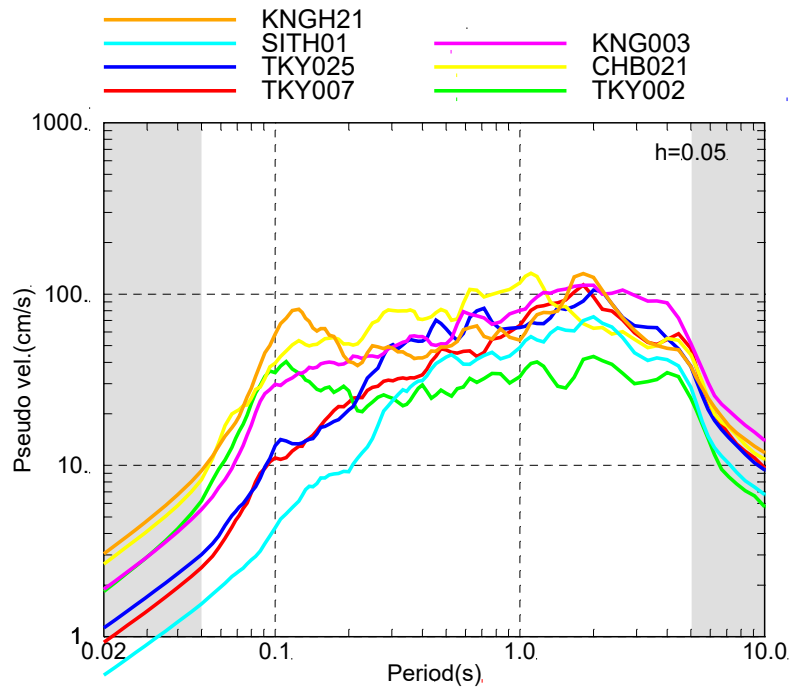


Fig. 7 – Pseudo velocity response spectra of strong ground motion simulations (damping ratio  $h = 0.05$ ). The seven sites are shown in color in Fig. 4, and these sites have relatively lower amplification factors than the remaining sites. Spectra were calculated by averaging the N-S and E-W components and the five rupture front fluctuation cases. The gray areas are outside the target periods.

#### 4. Conclusion

In this study, strong ground motion simulations of the 1923 Great Kanto earthquake in the Tokyo metropolitan area were conducted. Source characteristics were modeled by SMGA on the basis of the seismic intensity inversion analysis by Kanda and Kato [1]. Path and site characteristics were modeled on the basis of the inhomogeneous attenuation structure and the empirical amplification factors by Tomozawa and Kato [3]. Strong ground motion waveforms were generated using the stochastic Green's function.

The seismic intensity distribution of the simulation results was generally consistent with the distribution of observations based on the collapse rate of wooden houses [2]. For sites with relatively smaller empirical amplification factors, PGA was approximately 200 to 1000  $\text{cm/s}^2$ , and their response spectra levels were approximately 30 to 100  $\text{cm/s}$  at periods of approximately one to two seconds.

In this study, nonlinear site effects under large ground motions were not considered. Furthermore, the simulation sites and observation sites were not entirely in the same location. Therefore, studies are needed on nonlinear site effects and the spatial interpolation of empirical site amplification factors. These two topics represent the subjects for future research.

#### 5. Acknowledgments

We are grateful to Dr. Katsuhisa Kanda for the helpful comments and for providing data on seismic intensity inversion analysis and to Dr. Takashi Ikeda for the helpful comments on source modeling.

#### 6. Copyrights

Authors will have the right to use content of the published paper in part or in full for their own work.



## 7. References

- [1] Kanda K, Kato K (2019): SMGA and short-period spectral level of the historical earthquakes around Tokyo metropolitan area inferred from seismic intensity inversion. *Journal of JAEE (Special Issue)*, **19** (6), 91-104 (in Japanese).
- [2] Moroi T, Takemura M (2002): Re-evaluation on the damage statistics of wooden houses for the 1923 Kanto earthquake and its seismic intensity distribution in and around southern Kanto district. *Journal of JAEE*, **2** (3), 35-71 (in Japanese).
- [3] Tomozawa Y, Kato K (2018): Estimation of inhomogeneous attenuation structure of the Kanto region focusing on block division. *Summaries of technical papers of annual meeting, Architectural Institute of Japan*, 741-742, (in Japanese).
- [4] Irikura K (1986): Prediction of strong acceleration motion using empirical Green's function. *Proceedings of 7th Japan Earthq. Engr. Symp.*, 151-156.
- [5] Boore DM (1983): Stochastic simulation of high-frequency ground motions based on seismological models of the radiated spectra. *Bull. Seismol. Soc. Am.*, **73** (6A), 1865-1894.
- [6] Brune JN (1970): Tectonic stress and the spectra of seismic shear waves from earthquake. *J. Geophys. Res.*, **75** (26), 4997-5009.
- [7] Brune JN (1971): Correction. *J. Geophys. Res.*, **76**, 5002.
- [8] Eshelby JD (1957): The determination of the elastic field of an ellipsoidal inclusion, and related problems. *Proceedings of the Royal Society*, **A241** (1226), 376-396.
- [9] Disaster Management in Japan (2013): [http://www.bousai.go.jp/jishin/syuto/taisaku\\_wg/pdf/syuto\\_wg\\_report.pdf](http://www.bousai.go.jp/jishin/syuto/taisaku_wg/pdf/syuto_wg_report.pdf) (in Japanese).
- [10] The Headquarters for Earthquake Research Promotion (2009): "Map of long-period ground motions" Trial version in 2009, [https://www.jishin.go.jp/evaluation/seismic\\_hazard\\_map/lpshm/09\\_choshuki\\_dat/](https://www.jishin.go.jp/evaluation/seismic_hazard_map/lpshm/09_choshuki_dat/) (in Japanese).
- [11] Satoh T, Kawase H, Sato T (1994): Engineering bedrock waves obtained through the identification analysis based on borehole records and their statistical envelope characteristics. *Journal of Structural and Construction Engineering (Transactions of AIJ)*, **59** (461), 19-28 (in Japanese).
- [12] Boore DM, Boatwright J (1984): Average body-wave radiation coefficients. *Bull. Seismol. Soc. Am.*, **74** (5), 1615-1621.
- [13] Kato K, Hisada Y, Ohno S, Nobata A, Morikawa A, Yamamoto Y (2013): Benchmark tests for strong ground motion prediction methods: Case for stochastic Green's function method (Part 3). *AIJ Journal of Technology and Design*, **19** (41), 37-42 (in Japanese).
- [14] Sato H, Hirata N, Koketsu K, Okaya D, Abe S, Kobayashi R, Matsubara M, Iwasaki T, Ito T, Ikawa T, Kawanaka T, Kasahara K, Harder S (2005): Earthquake source fault beneath Tokyo. *Science*, **309** (5733), 462-464.
- [15] Kinoshita S (1993): Evaluation of site factor and propagation characteristics by means of earthquake observation. *Zisin*, **46**, 161-170 (in Japanese).
- [16] National Research Institute for Earth Science and Disaster Prevention (NIED): Strong-motion seismograph networks (K-NET, KiK-net), <http://www.kyoshin.bosai.go.jp/>.
- [17] Satoh T, Kawase H, Sato T (1994): Statistical spectral characteristics for engineering bedrock waves in which local site effects of surface geology are removed, Based on the ground motion records of small and medium earthquakes observed in the boreholes in Sendai. *Journal of Structural and Construction Engineering (Transactions of AIJ)*, **59** (462), 79-89 (in Japanese).